The Optical Dynamics of Excitons in Cylindrical J-Aggregates

S. S. Lampoura,[†,‡] C. Spitz,[§,#] S. Dähne,[§] J. Knoester,[†] and K. Duppen*[,†]

Materials Science Center, University of Groningen, Nijenborgh 4, 9747 AG Groningen, The Netherlands, Department of Biophysics and Physics of Complex Systems, Faculty of Sciences, Vrije Universiteit, De Boelelaan 1081, 1081 HV Amsterdam, The Netherlands, and Federal Institute for Materials Research and Testing, Richard-Willstaetter-Strasse 11, D-12489 Berlin, Germany.

Received: September 12, 2001; In Final Form: November 28, 2001

The optical dynamics of excitons in cylindrical 5,5′,6,6′-tetrachloro-1,1′-diethyl-3,3′−di(4-sulfobutyl)-benzimidazolocarbocyanine (TDBC)/C8O3 aggregates have been investigated by ultrafast pump−probe spectroscopy and accumulated photon echo experiments. In the nonlinear optical interactions, both the one-exciton band and the two-exciton band are excited. The interpretation of the results involves the separation of the two-exciton states into two types: those that have predominantly "ring"-character, with energy separations determined by the circumference of the cylinder, and those that have predominantly "longitudinal"-character, with energy separations determined by the coherence length of the excitons along the length of the cylinder. At 1.5 K, the excitons were found to be delocalized over an area of, on average, 95 molecules. These excitons can move incoherently to other localized regions on the cylinder, leading to rapid relaxation within the one-exciton band.

I. Introduction

The determination of the supramolecular structure of natural light-harvesting complexes (LHCs) of photosynthetic bacteria has stimulated renewed interest in the development of artificial light-harvesting systems. According to X-ray structure analysis, the LHC of the purple bacterium *Rhodopseudomonas acidophila* consists of highly symmetric ring systems formed by the self-organization of bacteriochlorophyll molecules in combination with various proteins.[1] Much theoretical and experimental work has been done on these circular structures.[2−15] Especially, the efficiency of the excitonic energy transport in these antenna systems has attracted much attention.[16−24] Studies on the optical dynamics of excitons in these natural aggregates provide inspiration for the search for artificial antenna systems.

To design artificial LHCs, self assembly of molecules has to occur in such a way that energy can be transferred efficiently from one molecule to another. These two guiding principles, self assembly and energy transport, are the main ingredients in the search for artificial systems with efficiencies that are comparable to those observed in natural antenna systems.

The self assembly of, for instance, surfactant-like molecules has been intensively investigated in the past decades.[25−27] By now, it is well-understood that hydrophobic interactions, hydrogen bonding, electrostatic and van der Waals interactions, and the rather weak coupling between π-electronic systems may all contribute to the driving forces that determine the self-organization of these amphiphilic surfactants. Additionally, steric requirements may play an important role.[28]

In contrast to these surfactant molecules, the driving force for self-organization of dye molecules, in particular of polymethine dyes,[29−33] is the strong intermolecular coupling caused by their very high optical polarizability, originating in molecular transitions with large dipoles. Interestingly, the size of these dipoles also helps such dye molecules to meet the requirement of efficient electronic energy transport, as they lead to strong intermolecular excitation transfer interactions. Strong transfer interactions give rise to collective eigenstates, in which many molecules share one single-molecule excitation. These one-excitation eigenstates form the so-called Frenkel exciton band. Similarly, two-, three-, and higher-exciton bands exist in which two, three, or more single-molecule excitations are present within the spatial extent of the delocalized excitations. Superradiant emission[34] and giant optical nonlinearities[35−38] are examples of optical phenomena that result from the collectivity in the response of molecular aggregates.

Because of their special properties, related to the strong electronic coupling, dye aggregates find many technological applications. They are used, for instance, as spectral sensitizers of photoinduced electron-transfer reactions in silver halide photography, as charge generation materials in electrophotography, and in nonlinear optical devices for information technology.[39] Their very high first and second hyperpolarizabilities allow for applications involving second and third harmonic generation and optical data storage.[39] They are also prime candidates in the development of artificial light-harvesting systems.

Self-assembled linear J-aggregates have been particularly well-studied over a large number of years.[31−33,40,41] In linear J-aggregates, the transition moments of the monomer units are more or less arranged parallel to each other with an angle of less than 54.7° (the magic angle) with respect to the aggregate axis. This gives rise to a Frenkel exciton band in which the optically allowed states are at the bottom of the energy spectrum.[42] Consequently, the observed absorption of the aggregates is red-shifted compared to that of the unaggregated

* To whom correspondence should be addressed. Tel: (31) 50 3634560. Fax: (31) 50 3634441. E-mail: k.duppen@chem.rug.nl.
† University of Groningen.
‡ Vrije Universiteit.
§ Federal Institute for Materials Research and Testing.
# New address: Institute of Physics, University of Potsdam, Am Neuen Palais, D-14415 Potsdam, Germany.

10.1021/jp013496v CCC: $22.00
Published on Web 03/06/2002

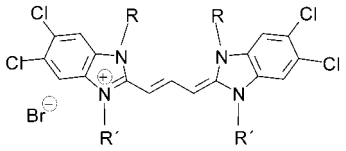

Figure 1. Chemical formulas of TDBC ($R = C_2H_5$; $R' = (CH_2)_4SO_3H$) and TDBC/C8O3 ($R = C_8H_{17}$; $R' = (CH_2)_3COOH$) dye molecules.

individual molecules. A single red-shifted and usually rather narrow J-band is observed when there is only one molecule per unit cell.

The structure of J-aggregates may be considerably more complicated than that of a simple linear molecular chain. When there are two or more translationally nonequivalent molecules in the unit cell, a split absorption band of two or more Davydov components is expected.[43] The splitting depends on the distance between the molecules, the magnitude of the electronic transition dipole moments involved in the coupling, and the angles of these transition dipole moments with respect to each other and the aggregate axis. For such aggregates with a unit cell composed of more than one molecule, different architectures have been proposed to account for the observed optical properties: helical structures, herringbone-like structures, and even zigzag angled chains.[44]

Recently, it was found that members of the family of 5,5′,6,6′-tetrachloro-1,1′-diethyl-3,3′di(4-sulfobutyl)-benzimidazolocarbocyanine (TDBC) molecules aggregate in different ways, subtly dependent on details of the molecular structure. The basic structure of TDBC molecules is shown in Figure 1. For TDBC itself (5,5′,6,6′-tetrachloro-1,1′-diethyl-3,3′di(4-sulfobutyl)benzimidazolocarbocyanine), the substituents are $R = C_2H_5$ and $R' = C_4H_8SO_3H$. When dissolved in water or water/ethylene glycol mixtures, even at very low concentrations, TDBC spontaneously and nearly completely aggregates due to strong intermolecular coupling, as evidenced from the large red shift of the J-band as well as the large free energy of association.[45] According to the appearance of a single sharp J-band, it is usually assumed that linear aggregate chains are formed with one molecule per unit cell. Because in cryogenic transmission electron micrographs (cryo-TEM) monolayer sheets are observed,[46] it is concluded that the interaction between chains is large enough to cause clustering but small enough not to influence the optical spectrum. By different methods, it was established that the "size" of the Frenkel exciton (the delocalization or coherence length of the excitations) is about 40 TDBC molecules for aggregates in an ethylene glycol/water glass at 1.5 K[47] and about 15 TDBC molecules for aggregates in room-temperature water.[48] Apparently, the intermolecular interactions in these aggregates are strong enough to counterbalance the perturbing influence of the ultrafast fluctuations of the water environment, which tend to localize the excitations.

A new type of TDBC J-aggregates is obtained when the aggregating molecules are made amphiphilic by substitution on one side with long hydrophobic alkyl groups and on the other side with hydrophilic acidopolymethylene groups. In this way, the ability of dye aggregates to transport energy is combined with the properties of surfactant-type molecules to form a variety of different supramolecular structures. These new types of aggregates were termed amphiPIPEs (*amphi*philes with *p*igment *i*nteractions *p*erforming *e*nergy migration).[49] An example of an amphiPIPE is TDBC/C8O3, in which the diethyl substituents are replaced by 1,1′-dioctyl groups and the disulfonyl substituents by 3,3′-di(carboxypropyl) groups (see Figure 1). The characterization of the excitonic level structure and the optical

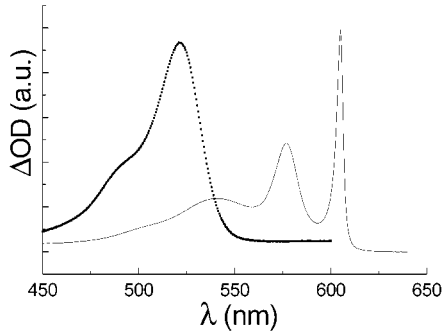

Figure 2. Absorption spectra of TDBC/C8O3. The dashed line is the monomer spectrum in methanol; the solid line is the aggregate spectrum in 10^{-2} M NaOH aqueous solution.

dynamics of supramolecular aggregates of this molecule are the main topics of this article. The absorption spectra of both the monomer and the aggregates of TDBC/C8O3 are shown in Figure 2.

The chemical substitutions on the side chains of TDBC, as described above, do not affect the spectral characteristics of the dye monomers. However, they induce strikingly different optical behavior in their J-aggregates because of the different supramolecular structures that are generated in the aggregation process.[50−55] For TDBC/C8O3, either superhelices[46] or, on addition of ionic surfactants, nanotubes or vesicles[56] are formed. As evidenced by the presence of J-absorption band(s) in the absorption spectrum, the intermolecular interactions are, to a large extent, still dominated by the strong coupling forces between the polymethinic molecules. However, the architecture of the aggregates is substantially modified by the amphiphilic nature of the substituents and their interaction with the environment via, for instance, hydrogen bonding and hydrophobic interactions.

Depending on the preparation conditions, the absorption spectrum of TDBC/C8O3 aggregates exhibits either a twofold[49−51,57] or a threefold split J-band.[49] This clearly suggests that two different types of supramolecular structures are possible. From ultrafiltration experiments, it turned out that the J-aggregates with a threefold split band are much larger ($\gg$0.2 μm) than those with a twofold split band ($<$0.2 μm).[58] Interestingly, both types of aggregates show optical activity in alkaline solutions, indicating spontaneous generation of chiral aggregates from TDBC/C8O3 molecules that are themselves achiral.[57] Originally, this effect was explained by the formation of herringbone-like J-aggregates with twisted side lobes.[57] Later, a helical supramolecular conformation was proposed.[51] After it was shown by spectroscopic measurements at high pressure that a hollow structure was likely,[53] a cylindrical geometry consisting of piled-up molecular rings was proposed as the most probable molecular arrangement in these aggregates. The structure of the J-aggregates with a threefold split J-band was visualized in cryo-TEM pictures, which proved their superhelical bilayered structure.[46] Hitherto, because of their much smaller size, the J-aggregates with a twofold split J-band could not be visualized by cryo-TEM.

The aggregate spectrum of Figure 2 shows two rather narrow peaks, at 604 and 575 nm, which on the basis of their polarization properties[49] have been identidied as the two exciton resonances that naturally occur in cylindrical aggregates (see section III). The broad structure at shorter wavelengths turns out to be unpolarized and is not attributed to an exciton transition;[49] its origin may be related to nonaggregated monomers or to vibronic transitions. The fact that the excitonic

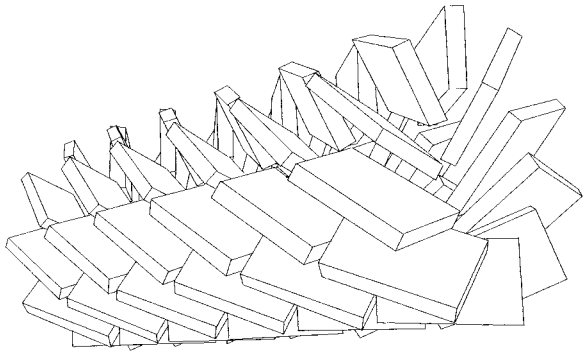

Figure 3. Artist's impression of a possible helical cylinder of TDBC/C8O3 aggregates. A box represents the plane of the molecular structure of the chromophores. In this example, the cylinder is divided into 10 helices, which are twined around each other. As will be discussed, it is more likely that the rings of molecules consist of only seven chromophores.

transition at 575 nm is considerably broader than the one at 604 nm may be attributed partly to fast relaxation from the higher-energy band into the lower-energy one. In addition, it has been shown that the effect of exchange narrowing is smaller by a factor of $\sqrt{2}$ for the higher exciton band compared to the lower one, as it derives from a transition that is degenerate in perfectly ordered aggregates.[59]

A possible molecular arrangement of the TDBC/C8O3 molecules in the aggregate with a twofold split absorption band is shown in Figure 3. This model combines a cylindrical shape with the helicity inferred from the observed optical activity. The inner region of the cylinder is formed by the hydrophobic octyl substituents, whereas the outer part of the cylinder makes the aggregates water-soluble because of the protuding carboxyl groups. The proposed cylindrical structure resembles that of the rod elements of the self-organized bacteriochlorophyll molecules in the chlorosomes of green bacteria.[60−62] The striking similarity between TDBC/C8O3 aggregates and these natural photosynthetic systems suggests that TDBC/C8O3 aggregates could make prominent candidates for future applications in artificial light-harvesting systems.

The linear optical properties of these aggregates were recently analyzed using a model of Frenkel excitons, which are distributed on the cylinder.[49] This yielded a cylinder circumference of about seven or eight molecules and a tilt angle of the molecular dipoles with a plane perpendicular to the cylinder axis in the range of 20°−32°. In the present paper, two time-domain nonlinear optical methods, pump−probe spectroscopy and accumulated photon echo experiments, are employed to investigate these aggregates further. The first technique provides information on the level of structure and the population dynamics of these cylindrical aggregates, while the second one probes the dephasing dynamics of the system. The results are discussed in the framework of a recent theory for the (non)-linear optical response of excitons in a cylindrical geometry, developed by Bednarz and Knoester.[63]

The paper is organized as follows: In section II, the sample handling and the experimental arrangements are described. A short introduction into the theory of excitons in cylindrical systems is given in section III. Subsequently, the experimental results are presented in section IV. Both static properties, such as the excitonic level structure and the spatial extent of the excitons, and dynamic properties, such as the exciton relaxation rate and the speed of propagation, are discussed. We summarize our conclusions in section V.

II. Materials and Methods

Samples were made by dissolving TDBC/C8O3[64] in distilled water containing NaOH by exposing it to ultrasonic waves for 10 s. Subsequently, the solution was mixed with ethylene glycol (EG) to produce a clear glass at low temperatures. The final solution had a concentration of 0.4 mM TDBC/C8O3 and 10 mM NaOH in a 80/20 vol % mixture of water/EG. A small amount of impurity from a precursor in the synthesis was also present. This did not influence the spectroscopic properties of the sample.

The cooling rate was found to influence the optical quality of the sample considerably. To minimize crystallization at low temperatures, the samples were rapidly immersed into a liquid nitrogen bath and then slowly cooled to 1.5 K. The measurements were exclusively performed in the available glassy area, which was about 40% of the sample surface. The optical density was set to 0.9−1.3 at the maximum of the aggregate absorption at 604 nm.

The laser system consisted of an Innova 99 mode-locked argon-ion laser, operating at 400 mW and generating pulses of 100 ps at a repetition rate of 94 MHz. These pulses were used to synchronously pump two dye lasers, containing rhodamine 6G in ethylene glycol as the lasing medium. A 16 cm focal length lens was employed to focus and cross the two collinear beams in the sample, which was located in an Oxford Research Instruments Variox variable-temperature optical cryostat. Pump−probe and accumulated photon echo experiments were performed in the wavelength range of 588−610 nm in the same way as described in ref 13.

In the pump−probe technique, the change in transmission of the probe pulse due to the influence of the pump pulse is measured as a function of the relative delay between these two pulses. The pump pulse transfers population from the electronic ground state to the excited state(s), so in general bleaching and stimulated emission is observed at the wavelengths of the ground-state transitions, while the absorption increases at wavelengths where excited-state transitions occur. The dynamics of these signals are governed by the time evolution of the populations of the various states involved.

In our experiments, one of the dye lasers generates the pump pulses and the other dye laser is used to generate the variably delayed probe pulses. The cross correlation of the dye lasers, as measured in a KDP crystal, was 10 ps, which is indicative of the time resolution of this technique. The laser power was kept below 0.2 mW for the pump beam and below 0.02 mW for the probe beam. When exciting at the red part of the absorption band, even at the lowest possible intensities with acceptable signal-to-noise ratio, some permanent bleaching of the sample was observed. Our reported results in section IV have been corrected for this photodamage.

For the accumulated photon echo (APE) experiments, a single dye laser was used. The laser beam was divided into two beams with equal intensity of 0.05 mW, with one of them variably delayed. The beam geometry was the same as in the pump−probe case: the two beams are crossed in the sample and the change in transmission of one beam due to the influence of the other beam is recorded. In this one-color experiment with phase-correlated pulses, the photon echo signal results from the scattering of the pump pulse in the direction of the probe pulse. This occurs through the interaction of the probe pulse with a population grating in frequency space. This grating is a modulation of the ground- and excited-state population as a function of the position in the (inhomogeneously broadened) spectrum. It is built up by the accumulated effect of many

pump−probe pulse pairs.[65,66] The signal is detected simultaneously with the one-color pump−probe signal, but under favorable conditions, the APE signal is significantly enhanced because of the accumulation effect. The dynamics of this signal are governed by the optical dephasing times of the transitions involved.

The APE experiments were performed using short, almost Fourier transform limited pulses with a duration of about 2 ps or much longer (10 ps) very broadband pulses with a very short correlation time. The observed dynamics were the same. The use of the latter method, that is, using stochastic fields for the excitation rather than fields with a well-defined optical phase, has some advantages. The time resolution of the APE experiments is determined by the field correlation time rather than by the duration of that field.[67] The 50 fs coherent spike of the autocorrelation signal, as measured in a KDP crystal, is indicative of the time resolution of the stochastic technique. The pulses with short correlation times were made by employing a 5 mm pellicle as the only wavelength tuning element in the dye laser.

The APE signal was in some cases a superposition of a pure APE signal and a broad pump−probe background. The use of stochastic excitation allows discrimination between both contributions because the APE signals grow with the field correlation of the pulses, while the pump−probe signal grows with the much broader intensity correlation.[13] Unequivocal identification of the signals can be made by scrambling the optical phase difference between consecutive pulse pairs. In that case, no accumulation of the signal can occur, leaving only the pump−probe signal. This scrambling can, for instance, be achieved by inserting a traveling wave modulator in one of the beams.[13,68] For all reported results of accumulated photon echo experiments, the signals were corrected for the pump−probe background.

A double modulation scheme was used for AM radio sideband detection of both pump−probe and accumulated photon echo signals to obtain a good signal-to-noise ratio even with very low laser powers.[69] Data handling and stepper-motor control for the variable delay were done with a computer. Absorption spectra were obtained using a broad band lamp and an optical multichannel analyzer.

III. Theory of Cylindrical Aggregates

Recently, a detailed model to describe the (non)linear optical response of excitons in cylindrical structures was developed by Bednarz and Knoester.[63] In this model, all molecules are equivalent and disorder in both the site energies and the intermolecular interactions is neglected (homogeneous aggregates). Here, we will briefly repeat, without going into detail, the most relevant aspects of this theory for the purpose of this article.

The Frenkel Hamiltonian, which describes the electronic states of molecules on a cylinder as two-level systems in the site representation, can be written as

$$H = E_{\mathrm{mol}} \sum_{\mathbf{n}} b_{\mathbf{n}}^{\dagger} b_{\mathbf{n}} + \sum_{\mathbf{n}} \sum_{\mathbf{m} \neq \mathbf{n}} J_{\mathbf{nm}} b_{\mathbf{n}}^{\dagger} b_{\mathbf{m}} \qquad (1)$$

where $b_{\mathbf{n}}^{\dagger}$ and $b_{\mathbf{n}}$ are Pauli creation and annihilation operators for (de)excitation on site $\mathbf{n}$, E_{mol} is the molecular two-level excitation energy, and $J_{\mathbf{nm}}$ is the excitation transfer interaction between molecules $\mathbf{n}$ and $\mathbf{m}$. The summations over $\mathbf{n}$ and $\mathbf{m}$ extend over the entire cylinder surface. These indices are two-dimensional vectors, $\mathbf{n} = (n_1, n_2)$ where $n_1 = 1, 2, ..., N_1$ and $n_2 = 1, 2, ..., N_2$.

The one-exciton eigenstates, in which the molecules on the cylinder share one single-molecule excitation, are

$$|\mathbf{q}\rangle = N^{-1/2} \sum_{\mathbf{n}} \mathrm{e}^{i\mathbf{q}\cdot\mathbf{n}} b_{\mathbf{n}}^{\dagger} |g\rangle \qquad (2)$$

where $\mathbf{q}$ is a Bloch wave vector with components $q_i = 2l_i/N_i$ along ($i = 1$) and around ($i = 2$) the cylinder, $l_i = 0, 1, ..., N_i - 1$, and $N = N_1 N_2$ is the total number of molecules on the cylinder. In the ground state $|g\rangle$ with energy $E_{\mathrm{g}} = 0$, all molecules are unexcited.

The properties of the one-exciton eigenstates of eq 2, including their eigenenergies, can be evaluated under general circumstances.[63] Here, for simplicity, we place the molecules on a rectangular lattice and take only nearest-neighbor interactions into account. In this way, all essential features of excitons in systems with a cylindrical geometry can be calculated analytically, including the properties of the two-exciton states (vide infra). The physical insight thus obtained can be refined later by numerical calculations for more complicated situations, such as the inclusion of longer-range interactions and disorder.

Under the conditions just described, the one-exciton energies read[63]

$$E_{\mathbf{q}} = E_{\mathrm{mol}} - 2J_1 \cos q_1 - 2J_2 \cos q_2 \qquad (3)$$

where J_1 and J_2 are the intermolecular nearest-neighbor couplings parallel to the cylinder axis and in a ring of molecules around this axis, respectively. When the transition probability from the ground state to the one-exciton band is evaluated, it is found that only three states are dipole-allowed. These are the transition from $|g\rangle$ to $|\mathbf{q}\rangle = |(0,0)\rangle$, which is polarized along the cylinder axis, and the two transitions from $|g\rangle$ to $|\mathbf{q}\rangle = |(0,\pm 2\pi/N_2)\rangle$, which are polarized perpendicular to the cylinder axis. The latter two transitions are degenerate so that, in general, two absorption features are expected for a homogeneous cylindrical aggregate. For oriented samples, these are polarized perpendicular to each other and they are separated by the energy

$$\Delta E = 2J_2(1 - \cos(2\pi/N_2)) \approx \frac{4\pi^2 J_2}{{N_2}^2} \qquad (4)$$

The approximate equality holds when N_2 is large enough.

When both J_1 and J_2 are positive, we are dealing with a JJ-aggregate (J aggregate character in both lattice directions). For nearest-neighbor transfer interactions, J_1 and J_2 of point dipole origin, this is only possible if the molecular dipoles make an angle with either one of the lattice directions that is between 54.7° and 35.3° (the magic angle and its complement). Including long-range interactions and (or) extended dipoles, however, may increase this range of orientations.[63] Because all experimental observations for TDBC/C8O3 aggregates, reported in section IV, are consistent with the situation of a JJ aggregate, we will here not consider the complications that arise in the nonlinear spectroscopy when one of the nearest-neighbor interactions is positive and the other negative, as is the case for HJ-aggregates.[63]

While the theory of the level structure and spectroscopy of the one-exciton band of cylindrical systems is a rather straightforward extension of the well-known cases of linear and circular aggregates, the states where the molecules on the cylinder share two excitations are not so easily derived. Yet, for nonlinear optical experiments such as pump−probe spectroscopy, transitions between the one-exciton band and the two-exciton band have to be considered. The complications arise from the Pauli

principle, which forbids double excitation of two-level molecules. Therefore, both excitations influence each other, even when dynamical interactions are ignored, as is usually done in the literature.

It is possible, however, to account for the Pauli exclusion interaction in the pump−probe spectrum without explicitly calculating the two-exciton states. This is done using the hard-core boson approach, in which the excitons are considered bosons that interact via a hard-core repulsion preventing them from occupying the same position.[70,71] The Green function for this situation, in which the hard-core potential acts like a delta-size scattering center in the relative position of the two excitations, can be evaluated exactly. This allows for the exact calculation of the pump−probe spectrum, using only information (wave functions and energies) of the one-exciton states.

In ref 63, the hard-core boson method was used to analyze the two-color pump−probe spectra of cylindrical aggregates as a function of various system parameters. One of the important results of this analysis is that for JJ aggregates the exact spectra are well-understood from an approximate set of two-exciton states. The main idea is to separate the two-exciton states into two classes: the first class, the intraring exciton states, contains those states in which both excitations reside in the same ring of the cylinder. The second set, the interring states, consists of those states in which both excitations reside on different rings. Although this separation does not yield the exact eigenstates, it can be shown that for JJ aggregates the approximation for the optically dominant states generally is very good.[63] Because, as stated above, we assume that we are dealing with JJ aggregates, we use this approximate set of two-exciton states to analyze the experimental spectra.

It is instructive to first consider the situation of a single-ring aggregate. In this case, we only have intraring two-exciton states. The level structure of the one- and the two-exciton bands and the transition dipole moments are well-known.[36,72] The lowest-energy transition from the ground state is shifted by an amount $2J_2$ compared to the single molecule energy: $E_{q=0} = E_{\mathrm{mol}} - 2J_2$. For the second excitation, the ring has effectively become smaller than that for the first one because of the Pauli exclusion principle that forbids two excitations to occupy the same site. Consequently, it takes more energy to put the second excitation on the ring than the first one, and therefore, the excited-state absorption occurs at a higher optical frequency. The difference between these two "ring" transitions is[63,72]

$$\Delta_{\mathrm{ring}} = 4J_2(1 - \cos(\pi/N_2)) \approx \frac{2\pi^2 J_2}{N_2^{\,2}} \qquad (5)$$

This is the energy separation between the induced absorption and bleaching features in the pump−probe spectrum of a ring J-aggregate when pumping the lowest ($q = 0$) one-exciton state (see section IV).

When many rings are stacked on top of each other to construct the cylinder, the basic picture of one-exciton formation is very similar: the bottom of the band shifts by an amount $2J_1$ compared to the ring frequency itself (see eq 3): $E_{q=0} = E_{\mathrm{mol}} - 2J_1 - 2J_2$. However, now two different classes of induced absorption transitions from the one-exciton band to the two-exciton band can be distinguished because the two-exciton states are separated into intraring and interring ones. For JJ-aggregates, both of them are blue-shifted compared to the lowest-energy transition from the ground state to the one-exciton band because of the Pauli exclusion principle. This blue shift is for the lowest-energy transition to the intraring two-exciton states given by[63]

$$\Delta_{\mathrm{intra}} = 4J_1 + 4J_2(1 - \cos(\pi/N_2)) \approx 4J_1 + \frac{2\pi^2 J_2}{N_2^{\,2}} \qquad (6)$$

where the term of $4J_1$ compared to eq 5 is due to the shift of the one-exciton band when the cylinder is formed. Similarly, the blue shift for the lowest-energy transition to the interring two-exciton band is

$$\Delta_{\mathrm{inter}} = 4J_1(1 - \cos(\pi/N_1)) \approx \frac{2\pi^2 J_1}{N_1^{\,2}} \qquad (7)$$

For more details concerning the separation into intra- and interring two-excitons states and their properties relevant to the pump−probe spectrum, the reader is referred to ref 63.

When the length of the cylinder, N_1, is larger than the circumference, N_2, and J_1 is comparable to or smaller than J_2, the transitions from the ground-state to the one-exciton levels and from the one-exciton levels to the "interring" two-exciton states have similar energy (eq 7), while the transition from the one-exciton levels to the "intraring" states occurs at much higher energy (eq 6). Thus, for rather narrow-band optical fields, simultaneous one- and two-photon resonances are only possible for the "interring" two-excitons. Also, the magnitudes of the "interring" and "intraring" nonlinear optical interactions are very different. The basic reason is that there are many more realizations for two excitations on different rings than for two excitations on a single ring. Consequently, the coherent (superradiant) behavior is particularly strong for the "interring" two-exciton states, and the corresponding transitions therefore dominate the nonlinear optical response. This picture is confirmed by the exact calculations of the nonlinear spectra, using the hard-core boson method.[63]

IV. Results and Discussion

The absorption spectrum of TDBC/C8O3, shown in Figure 2, exhibits two well-defined peaks (at 575 and 604 nm) and some weaker unresolved structure at higher energies. As discussed in section III, the explanation of this double-peak structure does not require the phenomenon of Davydov splitting, which arises because of the presence of more than one molecule per unit cell. Instead, our explanation is based on optical transitions that are polarized along and perpendicular to the cylinder axis, as is indeed observed in absorption experiments on oriented samples.[49] Because the two types of excitons differ only in their momentum around the cylinder axis (see the discussion following eq 3), the difference between their transition energies ΔE provides information on N_2 and J_2, that is, on the circumference of the cylinder and the intermolecular coupling in the direction around the cylinder axis. Using eq 4, we find $J_2/N_2^2 \approx \Delta E/(4\pi^2) = 21\ \mathrm{cm}^{-1}$ for the wavelengths of the two absorptions reported above.

In Figure 4, the pump−probe signals of TDBC/C8O3 aggregates at 1.5 K are displayed as a function of the probe wavelength for three different values of the pump wavelength. The traces are differential spectra, that is, the difference in the probe absorption spectrum with and without the pump pulse is plotted as a function of frequency. The dotted line is the absorption spectrum, which is in this energy range due to excitation from the ground state to the lowest-energy ($q = 0$) one-exciton state. The pump pulse creates population in the one-exciton band, which leads to bleaching of the ground state to

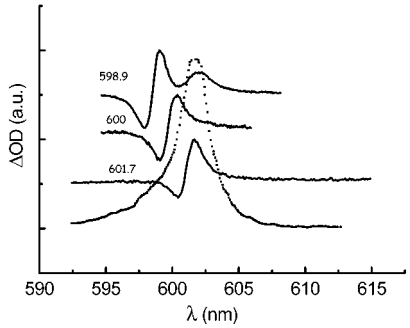

Figure 4. Pump−probe spectra of TDBC/C8O3 aggregates at 1.5 K for excitation wavelengths at 598.9, 600.0, and 601.7 nm. A positive deviation from the mean indicates bleaching (increased transmission of the probe due to the action of the pump), and a negative deviation indicates induced absorption. The dotted curve is the absorption spectrum at 1.5 K.

one-exciton transitions, stimulated emission from the excited one-exciton state to the ground state, and induced absorption at the frequency of the one-exciton to two-exciton transition(s). The former two effects lead to the positive features in the traces of Figure 4, while the induced absorption shows up as negative contributions in this spectrum. In these experiments, the pump and probe pulses are time coincident. The dynamics of the exciton states will be discussed below, when the results of time-resolved experiments will be presented.

As discussed in section III, in principle, two types of one-exciton to two-exciton transitions are expected: "intraring" and "interring" ones. However, the latter type of transition is expected to have much larger oscillator strength because of the fact that there are many more "interring" configurations of two-molecular excitations than "intraring" ones. So, the observed stimulated absorption in the pump−probe spectra of Figure 4 is due to the excitation of "interring" two excitons that are delocalized both along the circumference of the cylinder and also in the longitudinal direction. The energy difference between the pump pulse induced bleaching and induced absorption is therefore given by eq 7. For excitation at the center of the absorption band (the lowest trace of Figure 4), the application of eq 7 is straightforward. We find that $J_1/N_1^2 \approx \Delta E_{\text{inter}}/(2\pi^2) = 1.68\ \text{cm}^{-1}$ when the observed maxima of bleaching and absorption are taken as the energy difference. In fact, because of their overlapping profiles, the true energy separation between the two transitions is probably somewhat smaller. However, because the error made in this way is rather limited, we simply take the difference between the observed maxima as the correct value.

When the frequency of the pump pulse is changed to higher energy (middle and upper trace of Figure 4), the pump−probe spectrum shifts with it. This indicates that the absorption spectrum is inhomogeneously broadened. The difference between the maximum of the stimulated absorption and the main feature of the bleaching remains the same, implying that the inhomogeneity in the transition frequency does not affect the ratio J_1/N_1^2. At the highest pump energy shown in Figure 4, a second maximum in the bleaching develops at or near the center of the absorption band. In principle, this may result from the fact that in the cylinder direction periodic boundary conditions are not strictly valid, making higher-lying one-exciton states weakly dipole-allowed.[73] If such a state is excited by the pump pulse, not only the transition to this state but also the optically dominant lowest one-exciton transition is bleached. As the longitudinal cylinder size is an effective size determined by disorder (vide infra), it is difficult to make a quantitative check of this explanation. An alternative explanation is that, in the wing of the inhomogeneously broadened absorption band, the rather weak signals from the aggregates that are resonant with the pump pulse are comparable in intensity with the signals from the many aggregates at the center of the absorption band. The latter are excited off-resonantly in the wings of their homogeneous line shapes. As a result, the bleaching at the center part of the absorption band is comparable in magnitude to that in the blue wing of the inhomogeneous line shape. Model calculations indicate that this effect may only explain the second bleaching feature if we discard the contribution of the pronounced high-energy wing in the absorption band to the inhomogeneous contribution, that is, if we assume that this wing does not have excitonic character.

In addition to the ratios J_1/N_1^2, obtained from the pump−probe spectrum, and J_2/N_2^2, obtained from the linear absorption spectrum, there is one more spectral observation that provides information on the parameters of the excitons of the TDBC/C8O3 cylinders. This is the shift between the monomer absorption at 523 nm and the lowest-energy one-exciton absorption at 604 nm. According to eq 3 with $\mathbf{q} = (q_1,q_2) = (0,0)$, this difference is $2J_1 + 2J_2 = 2564\ \text{cm}^{-1}$. This relation, together with the two ratios mentioned above, provides insufficient information to unequivocally identify the values of all four parameters, N_1, N_2, J_1, and J_2. However, it is possible to establish these values within certain limits. For instance, from the three relations and the assumption of JJ-aggregates (both J_1 and J_2 are positive), it is easily deduced that $N_2 < 8$ should hold. When we assume in addition that it takes at least five molecules to build a ring, we find for the possible values of the excitonic parameters the following: (1) the number of molecules along the direction of the axis of the cylinder, $N_1 = 16 \pm 4$; (2) the number of molecules on the circumference of the cylinder, $N_2 = 6 \pm 1$; (3) the intermolecular coupling in the longitudinal direction, $J_1 = 500 \pm 250\ \text{cm}^{-1}$; (4) the intermolecular coupling in the circumferential direction, $J_2 = 800 \pm 250\ \text{cm}^{-1}$.

The uncertainties in the parameter values of the excitons are correlated. For instance, when we look at the surface size of the one-excitons, we find that the possible values are limited to the range $N_1N_2 = 95 \pm 10$. At the same time, it should be realized that additional uncertainty is caused by the fact that we deal with a simplified model, which only accounts for nearest-neighbor transfer interactions (see section III). Some insight into the effect of longer-ranging interactions was obtained in the analysis of ref 63, where point-dipole transfer interactions between the molecules were considered using an angle $\beta = 32°$ as additional experimental information. Not only nearest-neighbor interactions were taken into account, but also those between dipoles that are connected through the diagonal of the unit cell on the cylinder surface. This analysis yielded $N_1N_2 \approx 80$, with an uncertainty that resides in the angle β and the fact that the relative size of the two lattice constants is not exactly known. In view of the uncertainties mentioned, it is encouraging that the interpretation of these experiments, using entirely different assumptions concerning the interactions, yields very similar results for the number of molecules that participate in the excitation. We also note that the value for N_2 obtained above agrees with the estimate of seven or eight obtained from analyzing the linear absorption spectrum, assuming weak interactions in the longitudinal direction.[49]

The value of N_1N_2 does not necessarily reflect the size of the cylinder. In fact, the cryo-TEM pictures[46] of the TDBC/C8O3 aggregates with a threefold split J-band indicate a cylinder length of the order of micrometers, which is much longer than our

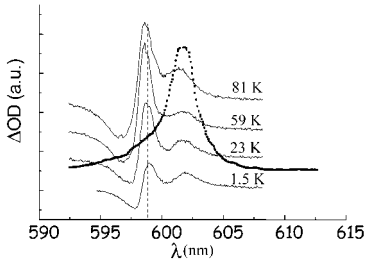

Figure 5. Pump−probe spectra of TDBC/C8O3 aggregates at four different temperatures, $T = 1.5$, 23, 59, and 81 K. As in Figure 4, a positive deviation from the mean indicates bleaching, while a negative deviation corresponds to induced absorption. The dashed line marks the excitation wavelength of 598.9 nm. The dotted curve is the absorption spectrum at 1.5 K.

estimate of N_1 implies. The reason is that, in the theory of section III, it was assumed that all monomers in the aggregate have exactly the same energy E_{mol} (eq 1). However, in reality, disorder is present in these energies or the intermolecular couplings J_1 and J_2, or both. This leads to localization of the excitons on a finite section of the cylinder.[45,73−75] The relative magnitude of the intermolecular coupling, compared to the energetic disorder, determines the degree of localization. The small value of N_2 in combination with the rather large intermolecular coupling, J_2, makes it very likely that N_2 is limited by the physical size of the circumference of the cylinder. This is consistent with the fact that the two J-bands in Figure 2 are spectrally well-separated. Moreover, the fact that the TDBC/C8O3 aggregates with a twofold split J-band cannot be resolved by cryo-TEM, suggests a very small cylinder diameter (<10 nm). However, N_1 probably is determined by the delocalization length of the excitons parallel to the cylinder axis, rather than the physical length of the cylinder.

The temperature dependence of the pump−probe spectrum allows for an independent determination of whether the physical size of the cylinder or disorder limits the value of N_1. For increasing temperatures, the excitons will scatter not only on static disorder but also on dynamic degrees of freedom such as phonons or vibrons ("dynamic disorder"). This limits the exciton coherence size to values smaller than the delocalization size imposed by static disorder (at 1.5 K, dynamic effects are not important and the two sizes are equal). As long as the coherence length in the longitudinal direction is larger than the length of the cylinder, no temperature dependence is expected in the experimental energy difference between stimulated absorption and bleaching, which is determined by J_1/N_1^2. In contrast, when the scattering on disorder is the determining factor, the energy separation between induced absorption and bleaching should grow with temperature, leading to a decreasing value of N_1 as extracted from experiment.[76,77]

In Figure 5, the temperature dependence of the pump−probe spectrum is shown. The bleaching remains more or less centered around the pump wavelength (the small shift is due to the increasing line width of the overlapping bleaching and absorption). However, the accompanying stimulated absorption clearly experiences an increasing blue shift when the temperature is raised, in accordance with the above expectations. When we assume that the intermolecular coupling constants J_1 and J_2 do not change over the temperature range of interest and that the coherence of the excitons along the circumference persists at all temperatures, we find that the excitons localize with temperature in a close to linear manner: $N_1N_2 \approx 95$ at 1.5 K, $N_1N_2 \approx 88$ at 23 K, $N_1N_2 \approx 77$ at 59 K, and $N_1N_2 \approx 69$ at 81 K. No detailed theory is currently available to explain this

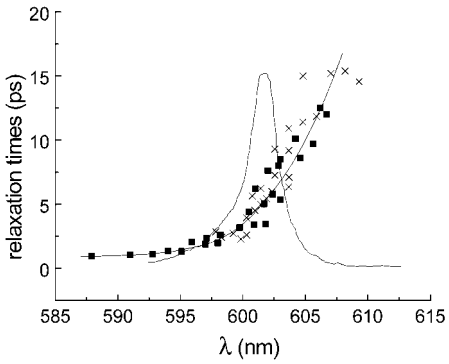

Figure 6. Population lifetime (×) and dephasing times (■) of TDBC/C8O3 aggregates as a function of wavelength at 1.5 K. The population lifetimes (T_1) were determined by single-exponential fitting of the decay of the bleaching part of pump−probe signals. The dephasing times ($^1/_2T_2$) were determined by single-exponential fitting of accumulated photon echo signals. The dashed line represents the optical density of the sample at 1.5 K, and the solid line is a guide to the eye.

behavior. The rate of decline of the size of the excitons with temperature seems to slow at higher temperature (not shown). However, because of the rapid increase in the line width of both bleaching and absorption, a more careful analysis than that presented here is required to extract the correct energy separation at higher temperatures.[48]

Now that it is clear that the physical size of the excitons of TDBC/C8O3 extends all around the cylinder, while along the longitudinal direction it is limited by static and (at elevated temperatures) dynamic disorder, it is interesting to discuss the dynamic properties of these excitons. Hence, the decay of the pump−probe signals as a function of the delay between the pump and probe pulses was recorded at $T = 1.5$ K. To the blue of 604 nm, single-color experiments were performed with pump and probe pulses derived from the same laser. In this way, the decay of the bleaching that is present at the frequency of the pump pulse is recorded. To the red of 604 nm, permanent photodamage of the sample made it difficult to perform such experiments reliably (see section II). To obtain information at those wavelengths, time-resolved two-color experiments were performed. The relatively strong pump pulse was applied at 599 nm, while the weak probe was varied over the second bleaching feature that exists in the red part of the pump−probe spectrum (see Figure 4). Thus, photodamage was kept to a minimum. In this way, the same decay times were recorded as with single-color experiments at the probe wavelength, but with improved reliability and accuracy.

At all wavelengths, the decay of the pump−probe signal could be fitted single-exponentially. The crosses in Figure 6 give the results of these fits as a function of probe wavelength. It is clear that the lifetime rapidly decreases when scanning from the very red side of the spectrum across the inhomogeneously broadened absorption band to the blue side. Such a trend indicates relaxation of the excitons through the one-exciton band. This is a phonon-assisted process that is associated with transport of excitons from one localized segment on the cylinder to another (incoherent hopping). Thus, the intraband relaxation that is observed in Figure 6 can be interpreted as propagation of localized excitons on a rugged energy landscape.

The time resolution in the two-color time-resolved pump−probe experiments (pumping in the blue and probing in the red) was not good enough to detect a rise in the signal due to the energy transfer from the blue to the red part of the spectrum. When we take the resolution to be 4 ps and also take into account that the exciton should at least propagate over one

delocalization length of $N_1 = 16$ molecules to find a lower energy position on the cylinder, we obtain four molecules per picosecond as the lower limit for the speed of propagation. Because high- and low-energy sites on the cylinder are probably farther apart than just one delocalization length, the real speed may be considerably higher. The upper limit, imposed by the J_1 value of 500 cm^{-1}, would be on the order of 70 molecules per picosecond, if the transport would be completely coherent. Such fast transport is only possible at low temperatures and limited to distances on the order of an exciton delocalization length. The translation of these numbers into the more conventional units of distance per unit time depends on the detailed geometry of the molecules in the cylinders.

In Figure 6, the optical dephasing times of the excitons, as measured in accumulated photon echo experiments, are shown as well (squares). When we take the two-level population relaxation parameter T_1 to be the decay time of the pump−probe signal and the two-level dephasing parameter T_2 to be the decay time of the photon echo experiment, we find that $T_1 = {}^1/_2T_2$ over the entire wavelength range. Using the well-known relation $(T_2)^{-1} = (2T_1)^{-1} + (T_2^*)^{-1}$, we find that the pure dephasing time $T_2^* = \infty$. Pure dephasing represents the phase relaxation of the excitation by modulation of the transition frequencies due to electron−phonon coupling or due to incoherent energy transfer between localization sites of (almost) equal energy. The absence of such effects at 1.5 K indicates that at low temperature the downhill hopping of the excitons toward lower energy regions on the cylinder is the only kind of energy transport that occurs. Energy transfer between localization sites of small energy difference (smaller than the spectral resolution of the experiment) would appear as a pure phase relaxation process, reflecting transport without an observable Stokes shift.

V. Conclusions

In this paper, we have studied the excitons of TDBC/C8O3 aggregates at different temperatures and excitation wavelengths. Both the linear and the nonlinear optical properties can be understood in terms of excitons on cylindrical structures. By combining data from the (linear) absorption spectra of the aggregates and monomers and the (nonlinear) pump−probe spectrum of the aggregates, the delocalization area of the excitons was established.

The diameter of the cylinder is the limiting factor in the number of molecules that are part of an exciton in the direction around the axis: 6 ± 1. Along the cylinder axis, energetic disorder limits the number of molecules that participates in the exciton to, on average, 16 ± 4 molecules. At $T = 1.5$ K, the delocalization area of the excitons was found to be 95 ± 10 molecules. This area decreased linearly with temperature between 1.5 and 81 K.

It should be realized that these numbers and their estimated errors are based on a simplified model, in which the molecules on the cylinder surface were placed on a rectangular lattice and only nearest-neighbor interactions were taken into account. In addition, the two-exciton states were separated into "intraring" and "interring" ones. Despite these approximations, the cited numbers give a fair indication of the nature of the excitons. As such, this paper is the first detailed experimental characterization of excitations on cylindrical structures.

Population relaxation and optical dephasing experiments showed that rapid relaxation occurs to the lowest-energy regions on the cylinders. Experiments with better time resolution are required to further study these processes. This type of energy relaxation is made possible by the rapid incoherent propagation of the excitons over the cylinder surface, even at the lowest available temperatures (1.5 K).

We end this paper by stressing that materials in which the excitons have a large delocalization area and a high speed of propagation over almost macroscopic ranges make promising candidates for artificial light-harvesting systems. We expect that self-assembled aggregates with cylindrical geometries, as discussed in this paper, will play an important role in future developments. Further research that is aimed at an increased understanding of the energy-transfer mechanisms and the energy-loss pathways is therefore required.

Acknowledgment. This work was supported by the Deutsche Forschungsgemeinschaft (Grants SFB 337, AB 74/5-3) and by the "Nederlandse Organisatie voor Wetenschappelijk Onderzoek" (NWO). INTAS (Grant 97-10434) is acknowledged for travel support enabling crucial discussions.

References and Notes

(1) McDermott, G.; Prince, S. M.; Freer, A. A.; Hawthornthwaite-Lawless, A. M.; Papiz, Z.; Cogdell, R. J.; Isaacs, N. W. *Nature* **1995**, *374*, 517.
(2) Bradforth, S. E.; Jimenez, R.; Van Mourik, F.; Van Grondelle, R.; Fleming, G. R. *J. Phys. Chem. B* **1995**, *99*, 16179.
(3) Novoderezhkin, V. I.; Razjivin, A. P. *Biophys. J.* **1995**, *68*, 1089.
(4) Sauer, K.; Cogdell, R. J.; Prince, S. M.; Freer, A.; Isaacs, N. W.; Scheer, H. *Photochem. Photobiol.* **1996**, *64*, 564.
(5) Pullerits, T.; Chachisvilis, M.; Sundström, V. *J. Phys. Chem.* **1996**, *100*, 10787.
(6) Alden, R. G.; Johnson, E.; Nagarajan, V.; Parson, W. W.; Law, C. J.; Cogdell, R. G. *J. Phys. Chem. B* **1997**, *101*, 4667.
(7) Koolhaas, M. H. C.; Van der Zwan, G.; Van Mourik, F.; Van Grondelle, R. *J. Phys. Chem. B* **1997**, *101*, 7262.
(8) Liuolia, V.; Valkunas, L.; Van Grondelle, R. *J. Phys. Chem. B* **1997**, *101*, 7343.
(9) Owen, G. M.; Hoff, A. J.; Jones, M. R. *J. Phys. Chem B* **1997**, *101*, 7197.
(10) Kühn, O.; Sundström, V. *J. Chem. Phys.* **1997**, *107*, 4154.
(11) Wu, H. M.; Rätsep, M.; Lee, I. J.; Cogdell, R. J.; Small, G. J. *J. Phys. Chem. B* **1997**, *101*, 7654.
(12) Wu, H. M.; Small, G. J. *J. Phys. Chem. B* **1998**, *102*, 63.
(13) Lampoura, S. S.; Van Grondelle, R.; Van Stokkum, I. H. M.; Cogdell, R. J.; Wiersma, D. A.; Duppen, K. *J. Phys. Chem. B* **2000**, *104*, 12072.
(14) Van Oijen, A. M.; Ketelaars, M.; Köhler, J.; Aartsma, T. J.; Schmidt, J. *Science* **1999**, *285*, 400.
(15) Mostovoy, M. V.; Knoester, J. *J. Phys. Chem. B* **2000**, *104*, 12355.
(16) Chachisvilis, M.; Kühn, O.; Pullerits, T.; Sundström, V. *J. Phys. Chem. B* **1997**, *101*, 7275.
(17) Jimenez, R.; Van Mourik, F.; Yu, J. Y.; Fleming, G. R. *J. Phys. Chem. B* **1997**, *101*, 7350.
(18) Kumble, R.; Hochstrasser, R. M. *J. Chem. Phys.* **1998**, *109*, 855.
(19) Krueger, B. P.; Scholes, G. D.; Fleming, G. R. *J. Phys. Chem. B* **1998**, *102*, 5378.
(20) Damjanović, A.; Ritz, T.; Schulten, K. *Phys. Rev. E* **1999**, *59*, 3293.
(21) Sundström, V.; Pullerits, T.; Van Grondelle, R. *J. Phys. Chem. B* **1999**, *103*, 2327.
(22) Leupold, D.; Stiel, H.; Ehlert, J.; Nowak, F.; Teuchner, K.; Voigt, B.; Bandilla, M.; Ücker, B.; Scheer, H. *Chem. Phys. Lett.* **1999**, *301*, 537.
(23) Mukai, K.; Abe, S.; Sumi, H. *J. Phys. Chem.* **1999**, *103*, 6096.
(24) Timpmann, K.; Woodbury, N. W.; Freiberg, A. *J. Phys. Chem. B* **2000**, *104*, 9769.
(25) Fuhrhop, J. H.; Köning, J. *Membranes and Molecular Assemblies: The Synkinetic Approach*; The Royal Society of Chemistry: Cambridge, U.K., 1994.
(26) Evans, D. F.; Wennerström, H. *The Colloidal Domain: Where Physics, Chemistry, Biology and Technology Meet*; VCH−Verlaggesellschaft: Weinheim, Germany, 1994.
(27) Lehn, J.-M. *Supramolecular Chemistry*; VCH−Verlaggesellschaft: Weinheim, Germany, 1995.
(28) Engelkamp, H.; Middelbeek, S.; Nolte, R. J. M. *Science* **1999**, *284*, 785.
(29) Dähne, S.; Nolte, K. D. *Chem. Commun.* **1972**, 1056.
(30) Stiel, H.; Dähne, S.; Teuchner, K. *J. Lumin.* **1988**, *39*, 351.
(31) Fidder, H.; Knoester, J.; Wiersma, D. A. *J. Chem. Phys.* **1993**, *98*, 6564.

(32) Minoshima, K.; Taiji, M.; Misawa, M.; Kobayashi, T. *Chem. Phys. Lett.* **1994**, *218*, 67.
(33) Kobayashi, T. *J-Aggregates*; World Scientific: Singapore, 1996.
(34) De Boer, S.; Vink, K. J.; Wiersma, D. A. *Chem. Phys. Lett.* **1987**, *137*, 99.
(35) Spano, F. C. *Phys. Rev. A* **1989**, *40*, 5783.
(36) Ishihara, H.; Cho, K. *Phys. Rev. B* **1990**, *42*, 1724.
(37) Bogdanov, V. L.; Viktorova, E. L.; Kulya, S. V.; Spiro, A. S. *Pis'ma Zh. Eksp. Teor. Fiz.* **1990**, *53*, 100 [*JETP Lett.* **1991**, *53*, 105].
(38) Knoester, J. *Chem. Phys. Lett* **1993**, *203*, 371.
(39) Bach, G.; Dähne, S. In *RODD's Chemistry of Carbon Compounds*; Sainsbury, M., Ed.; Elsevier Science: Amsterdam, 1997; Vol. IVB, Chapter 15.
(40) Jelley, E. E. *Nature* **1936**, *20*, 55.
(41) Scheibe, G. *Z. Elektrochem.* **1941**, *47*, 73.
(42) McRae, E. G.; Kasha, M. *J. Chem. Phys.* **1958**, *28*, 721.
(43) Davydov, A. S. *Theory of Molecular Excitons*; Plenum Press: New York, 1971.
(44) Daltrozzo, E.; Scheibe, G.; Gschwind, K.; Halmerl, F. *Photogr. Sci. Eng.* **1974**, *18*, 441.
(45) Makio, S.; Kanamura, N.; Tanaka, J. *Bull. Chem. Soc. Jpn.* **1980**, *53*, 3120.
(46) Von Berlepsch, H.; Böttcher, C.; Ouart, A.; Burger, C.; Dähne, S.; Kirstein, S. *J. Phys. Chem. B* **2000**, *104*, 5255.
(47) Moll, J.; Dähne, S.; Durrant, J. R.; Wiersma, D. A. *J. Chem. Phys.* **1995**, *102*, 6362.
(48) Van Burgel, M.; Wiersma, D. A.; Duppen, K. *J. Chem. Phys.* **1995**, *102*, 20.
(49) Spitz, C.; Knoester, J.; Ouart, A.; Dähne, S. *Chem. Phys.* **2002**, *275*, 271.
(50) Lindrum, M.; Dähne, S. *Phys. Status Solidi B* **1995**, *189*, 51.
(51) Pawlik, A.; Kirstein, S.; DeRossi, U.; Dähne, S. *J. Phys. Chem. B* **1997**, *101*, 5646.
(52) DeRossi, U.; Dähne, S.; Gomez, U.; Port, H. *Chem. Phys. Lett.* **1998**, *287*, 395.
(53) Spitz, C.; Dähne, S. *Ber. Bunsen-Ges. Phys. Chem.* **1998**, *102*, 738.
(54) Kirstein, S.; Von Berlepsch, H.; Böttcher, C.; Burger, C.; Ouart, A.; Reck, G.; Dähne, S. *ChemPhysChem* **2000**, 146.
(55) Spitz, C.; Dähne, S.; Ouart, A.; Abraham, H.-W. *J. Phys. Chem. B* **2000**, *104*, 8664.
(56) Von Berlepsch, H.; Böttcher, C.; Ouart, A.; Regenbrecht, M.; Akari, S.; Keiderling, U.; Schabblegger, H.; Dähne, S.; Kirstein, S. *Langmuir* **2000**, *16*, 5908.
(57) DeRossi, U.; Kriwanek, J.; Lisk, M.; Moll, J.; Spieles, M.; Bach, G.; Dähne, S. *J. Prakt. Chem.* **1995**, *3*, 203.
(58) Ouart, A. Thesis, Humbolt University, Germany, 2000 (http://dochost.rz.hu-berlin.de/dissertationen/ouart-andre-2000−09−28/PDF/Ouart.pdf).
(59) Didraga, C.; Knoester, J. *Chem. Phys.* **2002**, *275*, 307.
(60) Nozawa, T.; Ohtomo, K.; Suzuki, M.; Morishita, Y.; Madigan, M. T. *Bull. Chem. Soc. Jpn.* **1993**, *66*, 231.
(61) Nozawa, T.; Ohtomo, K.; Suzuki, M.; Nakagava, H.; Shikama, Y.; Konami, H.; Wang, Z. Y. *Photosynth. Res.* **1994**, *41*, 211.
(62) Prokhorenko, V. I.; Steengaard, D. B.; Holzwarth, A. R. *Biophys. J.* **2000**, *79*, 2105.
(63) Bednarz, M.; Knoester, J. *J. Phys. Chem. B* **2001**, *105*, 12913.
(64) The dye TDBC/C8O3 is available from FEW Chemicals, P.O. Box 1340, D-06756 Wolfen, Germany.
(65) Hesselink, W. H.; Wiersma, D. A. *Phys. Rev. Lett.* **1979**, *43*, 1991.
(66) Wiersma, D. A.; Duppen, K. *Science* **1987**, *237*, 1147.
(67) Asaka, S.; Nakatsuka, H.; Fujiwara, M.; Matsuoka, M. *Phys. Rev.* **1984**, *A29*, 2286.
(68) Hesselink, W. H. Thesis, University of Groningen, The Netherlands, 1980.
(69) Van Exter, M.; Lagendijk, A. *Rev. Sci. Instrum.* **1986**, *57*, 390.
(70) Leegwater, J. A.; Mukamel, S. *Phys. Rev. A* **1992**, *46*, 452.
(71) Juzeliūnas, G.; Knoester, J. *J. Chem. Phys.* **2000**, *112*, 2325.
(72) Spano, F. C. *J. Chem. Phys.* **1992**, *96*, 8109.
(73) Fidder, H.; Knoester, J.; Wiersma, D. A. *J. Chem. Phys.* **1991**, *95*, 7880.
(74) Schreiber, M.; Toyozawa, Y. *J. Phys. Soc. Jpn.* **1982**, *51*, 1537.
(75) Malyshev, V.; Moreno, P. *Phys. Rev. B* **1995**, *51*, 14587.
(76) Meier, T.; Chernyak, V.; Mukamel, S. *J. Phys. Chem. B* **1997**, *101*, 7332.
(77) Bakalis, L. D.; Knoester, J. *J. Phys. Chem. B* **1999**, *103*, 6620.